JOURNAL OF SOLID STATE CHEMISTRY 113, 398–404 (1994)

The New Perovskites $Sr_xLa_{2-x}CuTiO_{6-\delta}$, $BaLaCuTiO_{6-\delta}$, and Related Phases

S. Sefian-Lamarti, F. Weill, B. Darriet, P. Gravereau, and G. LeFlem

Laboratoire de Chimie du Solide du CNRS, Université Bordeaux I, 351 cours de la Libération, 33405 Talence Cedex, France

Received September 27, 1993; in revised form February 16, 1994; accepted March 16, 1994

The new perovskite $Sr_xLa_{2-x}CuTiO_{6-\delta}$ and some related phases, $Nd_2CuTiO_{6-\delta}$, $Gd_2CuTiO_{6-\delta}$, and $BaLaCuTiO_{6-\delta}$, have been identified. In the used experimental conditions, they contain specifically a high proportion of monovalent copper and oxygen vacancies. The structures of these materials, investigated using both X-ray diffraction and high resolution electron microscopy, are strongly related to the $GdFeO_3$ type structure. Copper titanium ordering will be discussed from the structural and physical properties. © 1994 Academic Press, Inc.

INTRODUCTION

Copper-rich oxides are largely used in various processes of heterogeneous catalysis (1, 2). The redox reaction $Cu^{2+} + e^- \rightarrow Cu^+$ (1), occuring in copper Nasicon type phosphates, has been correlated to the mechanism of oxidation of propene into acroleine. The same materials exhibit an oscillatory activity in the decomposition of 2-butanol (2). Since the matrix framework is covalent and zeolitic in nature, these catalytic properties are related to the high mobility of Cu^+ and the possibility of its reduction following by a nucleation of Cu(O) at the surface. In this case the relationship between catalytic activity and structure of the material have been clearly established.

In the perovskite-like matrices, the reaction (1) involves mobile lattice oxygen ions and this time, the catalytic properties are strongly dependent on the anion mobility and deficiency. Some perovskites have been tested for the production of oxygenated compounds from syngas ($CO + H_2$). Among these materials the $LaM_{0.5}Cu_{0.5}O_3$ (M = Ti, Mn) phases exhibit high methanol selectivity, but the actual composition and structure of the catalyst itself are not clearly established (3, 4). However, the subsolidus phase diagram of the La_2O_3–CuO–TiO_2 system in air at 960°C was recently published (5). The present paper reports a chemical and structure analysis of the $Sr_xLa_{2-x}CuTiO_{6-\delta}$ phase and of some related compounds. Described will be the material elaboration and an accurate determination of their composition, the structure evolution as a function of the composition, and the results of redox reaction models.

MATERIAL ELABORATION AND COMPOSITION

The following compounds have been prepared: $Ln_2CuTiO_{6-\delta}$ (Ln = La, Nd, Gd), $Sr_xLa_{2-x}CuTiO_{6-\delta}$ ($0 \leq x \leq 0.5$), and $BaLaCuTiO_{6-\delta}$.

To prepare $Sr_xLa_{2-x}CuTiO_{6-\delta}$, $Nd_2CuTiO_{6-\delta}$, and $Gd_2CuTiO_{6-\delta}$, mixtures of $Sr_xLa_{2-x}CuO_4$ (or Nd_2CuO_4, Gd_2CuO_4) and TiO_2 in stoichiometric ratio are ground together in a ball mill, pressed into pellets, and heated from 1050 (La(x = 0), Nd, Gd)] to 1200°C (x = 0.5) for 4 hr [La(x = 0) Nd, Gd)] to 2 days (x = 0.5) before a final quenching in air. This process avoids the formation of pyrochlore-related oxides ($Ln_2Ti_2O_7$) as impurities. The powders are deeply colored from ocher (Gd) to black (Sr, La).

For the preparation of $BaLaCuTiO_{6-\delta}$ the starting oxides were BaO_2, CuO, and TiO_2. A mixture at the stoichiometric ratio was heated at 900°C for 15 hr and then at 950°C for 15 hr with intermediate grinding before a final quenching in air. The color of the powder was black.

Various techniques were used to determine the composition:

(i) Electron probe microanalysis checked the preservation of the cationic ratios (Ln/Sr)/Cu and Cu/Ti. Imaging displayed the homogeneous distribution of the cations within given samples.

(ii) The oxidation state of copper was determined by iodometric titration using a concentrated KI solution. The results were corroborated by measuring the thermal evolution of the magnetic susceptibilities.

(iii) Under the above-described experimental conditions significant weight losses were observed but no Ti^{3+} EPR signal was detected. Therefore the final oxidation states of transition ions were assumed to be Ti^{4+}, Cu^+, and Cu^{2+}, involving the general formula

$$Ln_2TiCu_y^{2+}Cu_{1-y}^{+}O_{(11+y)/2}$$

0022-4596/94 $6.00

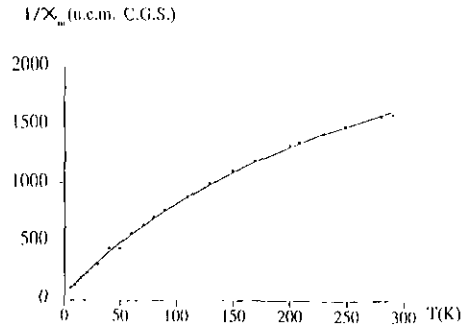

FIG. 1. Thermal variation of the reciprocal magnetic susceptibility of $La_2CuTiO_{6-\delta}$.

$$Sr_xLa_{2-x}TiCu_y^{2+}Cu_{1-y}^{+}O_{(11+y-x)/2}$$

and

$$BaLaTiCu_y^{2+}Cu_{1-y}^{+}O_{(10+y)/2}.$$

For all the compounds the chemical analysis gives a constant value of $y = 0.25 \pm 0.02$, except for the barium oxide, for which $y = 0.22 \pm 0.02$.

The magnetic susceptibilities of the lanthanum oxides were measured. An example is given in Fig. 1, which shows $\chi_M^{-1} = f(T)$ for $La_2CuTiO_{6-\delta}$.

All the curves are typical of Cu^{2+} paramagnetism: a straight line is observed at low temperature and then the curve becomes progressively concave toward the T axis. This evolution results from the increasing influence of the temperature independent paramagnetism (TIP) and precludes magnetic interaction between Cu^{2+}'s nearest neighbors. The magnetic curves fit the equations:

$$\chi_{La_2CuTiO_{6-\delta}} = \frac{0.0947}{T} + 295 \times 10^{-6} \text{ emu cgs}$$

$$\chi_{Sr_{0.25}La_{1.75}CuTiO_{6-\delta}} = \frac{0.0979}{T} + 235 \times 10^{-6} \text{ emu cgs}$$

$$\chi_{Sr_{0.5}La_{1.5}CuTiO_{6-\delta}} = \frac{0.0982}{T} + 250 \times 10^{-6} \text{ emu cgs}$$

$$\chi_{BaLaCuTiO_{6-\delta}} = \frac{0.078}{T} + 216 \times 10^{-6} \text{ emu cgs}.$$

The Curie constants are close to the value corresponding to $y = 1/4$ (Ba $y = 0.21$), assuming a spin only contribution ($C_{cal} = 0.09375$).

Therefore the magnetic data are strongly consistent with the results of the chemical analysis. All samples contain titanium (IV), copper (I), and copper (II). The Cu^{2+}/Cu^{+} ratio is 0.33, except for the barium compound, in which this ratio is equal to 0.28. Strontium and barium enrichment increase the number of oxygen vacancies without modifying the cation oxidation states. Accordingly the formulae of the as-prepared materials are $Ln_2CuTiO_{5.625}$($x = 0$), $Sr_{0.25}La_{1.75}CuTiO_{5.5}$($x = 0.25$), $Sr_{0.5}La_{1.5}CuTiO_{5.375}$($x = 0.5$), and $BaLaCuTiO_{5.11}$($x = 1$).

TABLE 1
Conditions Used for Data Collection

Sample container	Aluminum holder
Diffractometer	Philips PW 1820
Monochromator	Graphite
Instrument geometry	Bragg Brentano
Wavelength λ(Å)	$K\alpha_{1-2}Cu \left[\frac{I_{K\alpha_2}}{I_{K\alpha_1}} = 0.50\right]$
Data collection range (2θ)	15–110
2θ step (°)	0.02
Refinement program	DBW 3.2S (6)
Law for full-width at half maximum (FWHM)	Law of Caglioti: $H^2 = U \tan^2\theta + V \tan\theta + W$
Analytic function for profile shape	Pseudo-Voight (PV): $PV = \eta L + (1 - \eta)G$
Background	Polynomial function

CRYSTAL STRUCTURE

The structures of the lanthanum compounds have been tentatively determined using a Rietveld refinement of their X-ray powder diffraction data and a high resolution transmission electron microscopic analysis.

X-Ray Diffraction Investigation

The conditions used for the data collection are given in Tables 1 and 2.

The order of magnitude of the parameters involves a $GdFeO_3$ type structure. The RT X-ray powder diffraction of all samples (except Ba) could be indexed using an orthorhombic (0) cell derived from a simple cubic (c) perovskite: $a_0 \simeq \sqrt{2}\, a_c$, $b_0 = \sqrt{2}\, a_c$, $c_0 = 2a_c$ (Table 3). The symmetry of $BaLaCuTiO_{6-\delta}$ is cubic with $a_c = 3.941 \pm 0.001$ Å. The unit cell volume decreases as the

TABLE 2
Reitveld Refinement Results (space group *Pbmn* $Z = 2$)

Compound	Number of reflections	Number of refined parameters	R_p	R_{wp}	R_I
$La_2CuTiO_{6-\delta}$	138	27	0.049	0.0653	0.0356
$Sr_{0.25}La_{1.75}CuTiO_{6-\delta}$	166	27	0.0451	0.059	0.0379
$Sr_{0.5}La_{1.5}CuTiO_{6-\delta}$	165	23	0.0512	0.0718	0.0562

TABLE 3
Unit Cell Parameters (Å) and Volumes (Å^3)

Compound	$a \pm 0.001$	$b \pm 0.001$	$c \pm 0.001$	a_c	$V \pm 0.2$
$La_2CuTiO_{6-\delta}$	5.570	5.601	7.851	3.941	244.8
$Nd_2CuTiO_{6-\delta}$	5.475	5.733	7.643	3.914	239.8
$Gd_2CuTiO_{6-\delta}$	5.363	5.515	7.515	3.868	231.5
$Sr_{0.25}La_{1.75}CuTiO_{6-\delta}$	5.579	5.579	7.870	3.942	244.9
$Sr_{0.5}La_{1.5}CuTiO_{6-\delta}$	5.554	5.554	7.854	3.927	242.3
$BaLaCuTiO_{6-\delta}$				3.942	61.3 ($Z = 1$)

rare earth sizes decrease. The substitution of strontium or barium for lanthanum involves a decrease of the distortion from cubic symmetry and finally a cubic cell is observed for $BaLaCuTiO_{6-\delta}$.

The densities were carefully measured by the hydrostatic method in connection with estimation of the oxygen deficiency. In Table 4, the experimental results are compared with the d_1 values calculated for the hypothetical stoichiometric composition (O_6 formula) and with the d_2 values obtained for compositions deduced from chemical analysis and magnetic measurements. Within the experimental error deviations, the measured densities are in agreement with the formulae given above.

Charge differences between Ti^{4+} and Cu^+ or Cu^{2+} should indicate an ordered arrangement in the octahedral sites of the structure. Attempts to refine the crystal structures of the $Sr_xLa_{2-x}CuTiO_{6-\delta}$ compounds by the Rietveld method using the $P2_1/n$ space group (7, 8), which permits such an ordering, was unsuccessful. Therefore a tentative refinement within the context of the *Pbnm* space group was carried out. The structure of $LaFeO_3$ was used as a trial model (9). As a general trend, a random distribution of oxygen vacancies over the two possible oxygen sites (labelled O_1 and O_2) leads to an increase of the R factors. The best refinements were obtained by fixing the vacancy only at the O_1 position, with the occupancy factor deduced

TABLE 4
Comparison of the Experimental and Calculated Densities Corresponding to an (O_6) Formula and to the Results of the Chemical and Thermomagnetic Analysis

Compound	$d_{exp.}$(Mg cm^{-3}) ±0.07	d_1(Mg cm^{-3})	d_2(Mg cm^{-3})
$La_2CuTiO_{6-\delta}$	6.42	6.59	6.508
$Nd_2CuTiO_{6-\delta}$	6.78	6.868	6.785
$Gd_2CuTiO_{6-\delta}$	7.42	7.486	7.40
$Sr_{0.25}La_{1.75}CuTiO_{6-\delta}$	6.29	6.405	6.296
$Sr_{0.5}La_{1.5}CuTiO_{6-\delta}$	6.18	6.438	6.163
$BaLaCuTiO_{6-\delta}$	6.26	6.56	6.33

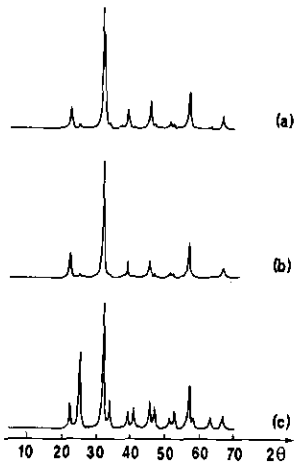

FIG. 2. XRD patterns of $La_2CuTiO_{6-\delta}$: (a) experimental, (b) simulation with the space group *Pbmn*, (c) simulation with the space group $P\,2_1/n$.

from the chemical analysis. Due to their strong correlations with the occupancy factors, the thermal B parameters were fixed with realistic values (Fig. 2).

Figure 3 gives as an example the observed and difference X-ray powder diffraction profiles of $Sr_{0.5}La_{1.5}CuTiO_{6-\delta}$. Table 5 gives the final atomic positions. The X-ray diffractogram of $BaLaCuTiO_{6-\delta}$ is consistent with the *Pm3m* space group of $CaTiO_3$. Table 6 gives selected bond lengths for both octahedral and La/BaSr sites.

These materials can be described as anion-deficient perovskites with a random distribution of copper and titanium over the octahedral sites. The oxygen vacancies seem to be located only in the apical position (O_1) of the octahedron. The refinement of the diffraction data cannot account for possible small atomic displacements around this defect. Increasing the proportion of strontium or barium increases the unit cell symmetry and simultaneously moves the atomic coordinates to the typical values associ-

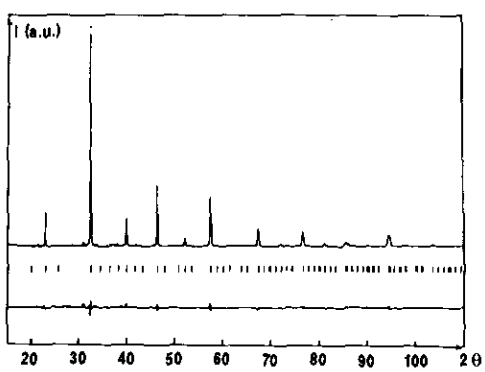

FIG. 3. Observed, calculated, and difference X-ray powder diffraction patterns of $Sr_{0.5}La_{1.5}CuTiO_{6-\delta}$.

TABLE 5
Final Atomic Positions and Thermal Atomic Parameters for the $Sr_xLa_{2-x}CuTiO_{6-\delta}$ Phase

Atoms	Site	x	y	z	B_{iso}(Å)	Occupancy
$La_2CuTiO_{6-\delta}$						
La	4c	0.0057(04)	0.0356(01)	0.25	0.9	2
Cu/Ti	4b	0.5	0	0	0.4	1
O_1	4c	0.9727(26)	0.4843(15)	0.25	1	1.825
O_2	8d	0.2858(19)	0.2795(17)	0.0398(10)	1	4
$Sr_{0.25}La_{1.75}CuTiO_{6-\delta}$						
Sr/La	4c	0.040(07)	0.0268(02)	0.25	0.5	2
Cu/Ti	4b	0.5	0	0	0.5	1
O_1	4c	0.9263(49)	0.4950(24)	0.25	1	1.5
O_2	8d	0.2736(39)	0.2774(37)	0.0262(29)	1	4
$Sr_{0.5}La_{1.5}CuTiO_{6-\delta}$						
Sr/La	4c	−0.0056(05)	0.0096(04)	0.25	0.5	2
Cu/Ti	4b	0.5	0	0	0.5	1
O_1	4c	0.9712(11)	0.4960(48)	0.25	1	1.375
O_2	8d	0.2593(63)	0.2548(67)	0.0382(16)	1	4

ated with the ideal cubic perovskite atomic positions. Obviously, such an investigation cannot distinguish the actual local symmetry of Cu^+, Cu^{2+}, or Ti^{4+}. Their statistical distribution must be understood at long range.

TABLE 6
Selected Bond Lengths (Å) for the $Sr_xLa_{2-x}CuTiO_{6-\delta}$ and $BaLaCuTiO_{6-\delta}$ Phases

	Octahedral site		Deodecahedral site	
$La_2CuTiO_{6-\delta}$	Cu/Ti-O_1	= 2.011 × 2	La-O_1	= 2.403
				= 2.555
				= 3.120
				= 3.196
	Cu/Ti-O_2	= 1.993 × 2		
			La-O_2	= 2.475 × 2
	Cu/Ti-O_2	= 2.039 × 2		= 2.650 × 2
				= 2.783 × 2
	⟨Cu/Ti-O⟩	= 2.014		= 3.305 × 2
$Sr_{0.25}La_{1.75}CuTiO_{6-\delta}$	Cu/Ti-O_1	= 2.042 × 2	La/Sr-O_1	= 2.625
	Cu/Ti-O_2	= 1.986 × 2		= 2.671
	Cu/Ti-O_2	= 2.010 × 2		= 3.020
	⟨Cu/Ti-O⟩	= 2.012		= 3.026
			La/Sr-O_2	= 2.541 × 2
				= 2.710 × 2
				= 2.75 × 2
				= 3.192 × 2
$Sr_{0.5}La_{1.5}CuTiO_{6-\delta}$	Cu/Ti-O_1	= 1.966 × 2	La/Sr-O_1	= 2.656
	Cu/Ti-O_2	= 1.968 × 2		= 2.707
	Cu/Ti-O_2	= 1.999 × 2		= 2.847
	⟨Cu/Ti-O⟩	= 1.977		= 2.847
			La/Sr-O_2	= 2.603 × 2
				= 2.609 × 2
				= 2.911 × 2
				= 3.021 × 2
$BaLaCuTiO_{6-\delta}$	Cu/Ti-O	= 1.971 × 6	Ba/La-O	= 2.786 × 12

High Resolution Transmission Electron Microscopy Analysis

High resolution transmission electron microscopy, coupled with selected area electron diffraction, has been used to determine possible ordering schemes. For the investigated samples, i.e., $La_2CuTiO_{6-\delta}$, $Sr_{0.25}La_{1.75}CuTiO_{6-\delta}$, and $Sr_{0.5}La_{1.5}CuTiO_{6-\delta}$,

(i) High resolution images reveal the absence of any microscopic defects or apparent microdomains (Fig. 4).

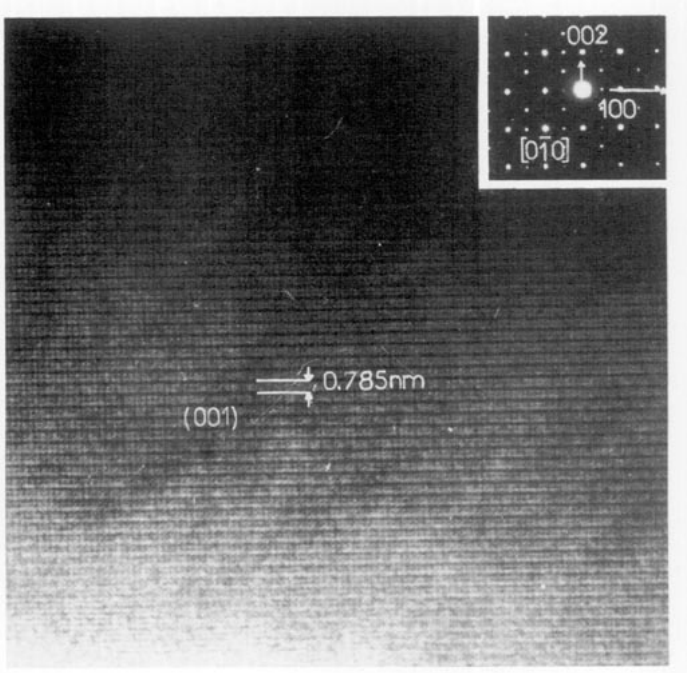

FIG. 4. An image of a $La_2CuTiO_{6-\delta}$ microcrystal.

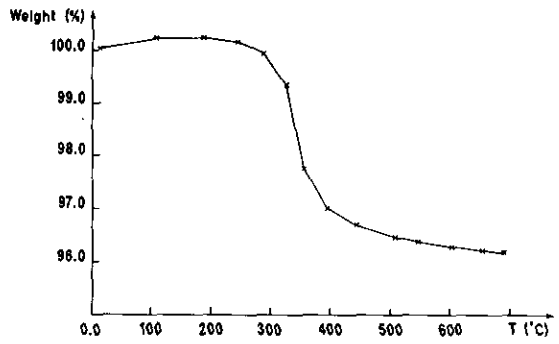

FIG. 5. Thermogravimetric analysis of $La_2CuTiO_{6-\delta}$ under a flow of 90% argon, 10% hydrogen.

(ii) The electron diffraction patterns can be indexed assuming a pseudo-cubic cell of parameters $\simeq 2a_c$. This new cell is a superstructure of the previous ones. New refinements from the X-ray diffraction data lead to the following parameters:

for $La_2CuTiO_{6-\delta}$

$$a = b = 7.898 \pm 0.001 \text{ Å}$$
$$c = 7.850 \pm 0.001 \text{ Å}$$
$$\gamma = 90.32°$$

for $Sr_{0.25}La_{1.75}CuTiO_{6-\delta}$

$$a = b = 7.890 \pm 0.001 \text{ Å}$$
$$c = 7.870 \pm 0.001 \text{ Å}$$

for $Sr_{0.5}La_{1.5}CuTiO_{6-\delta}$

$$a = b = 7.855 \pm 0.001 \text{ Å}$$
$$c = 7.870 \pm 0.01 \text{ Å}.$$

Such results are consistent with a Cu/Ti short range order. In addition, the absence of extended defects can presumably be related to a low degree of vacancy mobility.

OXIDATION–REDUCTION REACTIONS

With respect to possible use of these oxides as catalysts, preliminary experiments with reduction and oxidation reactions have been carried out. The investigated oxides were $Ln_2CuTiO_{6-\delta}$ (Ln = La, Nd) and $Sr_{0.25}La_{1.75}CuTiO_{6-\delta}$.

Reduction Reactions

The reduction of the samples was brought about by heating the as-prepared powders under a flow of 10% H_2, 90% Ar from RT to 700°C (200°C/hr). As an example, the reduction of $La_2CuTiO_{6-\delta}$ begins at 300°C (Fig. 5) and under the experimental conditions, the weight loss maximum, about 4%, is reached at 700°C. The XRD patterns of the reduced sample shows

—copper metal

—a cubic perovskite like phase whose parameter (a = 3.949 ± 0.001 Å) is between the parameters of the equiva-

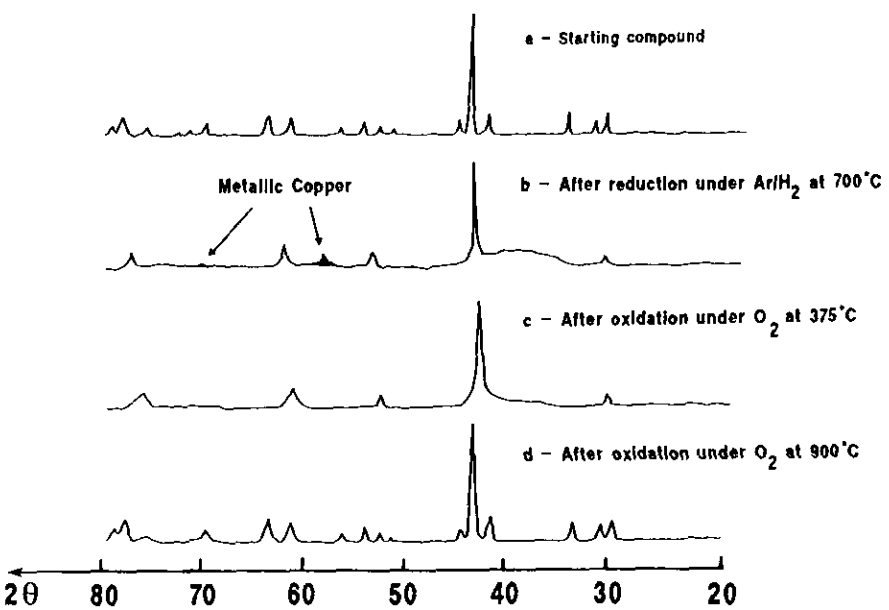

FIG. 6. XRD patterns observed during a cycle of oxidation-reduction for $Nd_2CuTiO_{6-\delta}$.

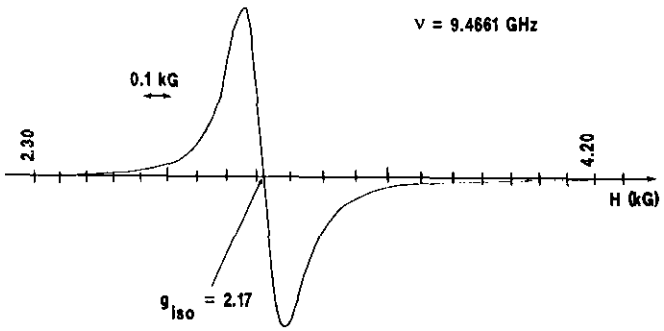

FIG. 7. EPR signal of $Sr_{0.5}La_{1.5}CuTiO_{6-\delta}$ at T = 4.2 K.

lent cubic cells of $LaTiO_3$ (a = 3.956 Å) (10) and $La_2CuTiO_{6-\delta}$ (a = 3.944 Å)

—the main lines of $La_2Ti_2O_7$ and La_2TiO_5.

For $Sr_{0.25}La_{1.75}CuTiO_{6-\delta}$ the copper metal appears at 300°C, but the X-ray pattern of the starting material is still preserved until 400°C, at which temperature an orthorhombic → cubic transition occurs (a_c = 3.946 Å). In both cases EPR spectra evidence the presence of Ti^{3+}. The paramagnetic susceptibilities and the electronic conductivity are weak.

Oxidation Reactions

The reduced samples were annealed under a dry oxygen flow at 450–500°C and then at 950°C. At 450–500°C the copper metal is no longer detected, whereas the XRD pattern exhibits a unique cubic perovskite phase with rather broad lines (e.g., a = 3.970 ± 0.001 Å for $La_2CuTiO_{6-\delta}$). At this stage only the isotropic EPR signal of Cu^{2+} was observed. Chemical analysis and magnetic measurements indicate a Cu^{2+} proportion of 20%. At higher temperature the starting materials are completely restored from a structural point of view and also with regard to composition (25% Cu^{2+}). These evolutions are illustrated in Fig. 6, which exhibits the XRD patterns recorded during a total oxidation–reduction cycle for $Nd_2CuTiO_{6-\delta}$. In conclusion, copper atoms can reversibly leave the structure as metal by a mechanism which must be investigated at length.

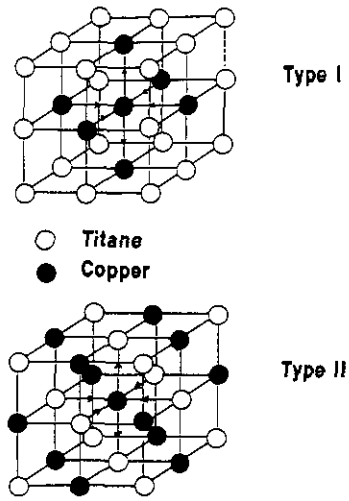

FIG. 9. Hypothetical copper–titanium ordering in $Sr_xLa_{2-x}CuTiO_{6-\delta}$: (a) Type I, (b) Type II.

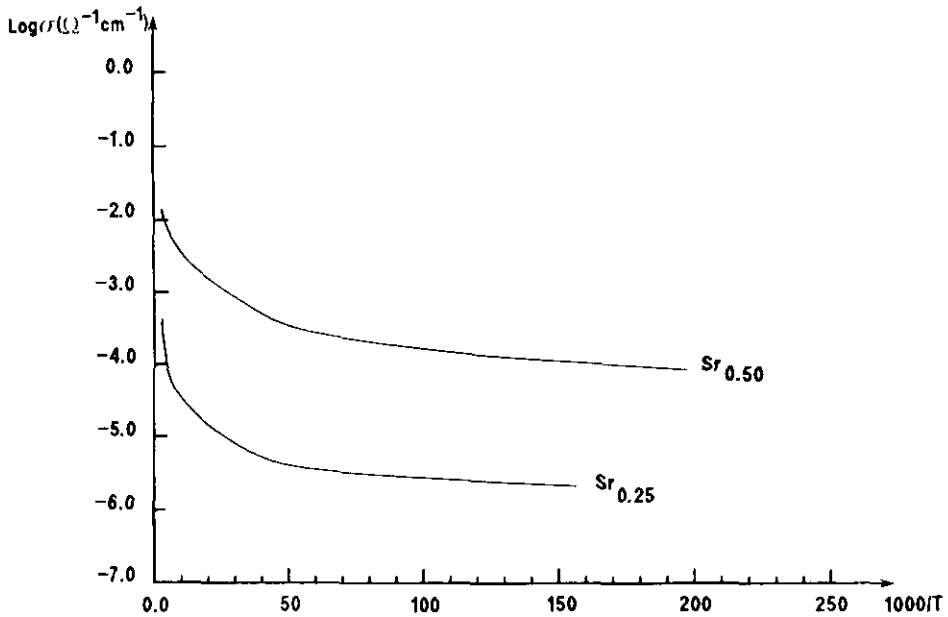

FIG. 8. Thermal variation of the electronic conductivity of $Sr_{0.25}La_{1.75}CuTiO_{6-\delta}$ and $Sr_{0.5}La_{1.5}CuTiO_{6-\delta}$.

DISCUSSION AND CONCLUSIONS

A better insight into the copper (II) environment is given by EPR spectroscopy. The signals recorded at 4.2 K for all the compounds of the $Sr_xLa_{2-x}CuTiO_{6-\delta}$ solid solution are remarkably isotropic (g = 2.17) (Fig. 7), which is unexpected for a Cu^{2+} site distorted by a static Jahn–Teller effect. Nevertheless, an identical signal (g = 2.197) was reported at RT for $Ba_3CuSb_2O_9$ of the elpasolite type structure. The copper (II) site is then an almost regular octahedron (11). Conversely, a static Jahn–Teller effect at the Cu(II) site of $BaLaCuTiO_{6-\delta}$ can be deduced from the EPR signal recorded at 4.2 K: $g_{\parallel}$ = 2.397 and $g_{\perp}$ = 2.076. These data can be compared with those reported for Cu^{2+} in $Sr_2CuW_2O_9$ ($g_{\perp}$ = 2.44, $g_{\parallel}$ = 2.08), where the CuO_6 entities are statistically distorted (12).

These results demonstrate, at least for the LaSr phase, the uniqueness of the copper (II) site and the absence of vacancies in the first coordination shell. The symmetry of $BaLaCuTiO_{6-\delta}$ is probably lower at low temperatures.

A possible model of Cu/Ti ordering can be deduced from the previous group of data:

(i) A constant Cu^+/Cu^{2+} ratio has been determined by two very different techniques, chemical analysis and magnetic measurements. This suggests the existence of a small entity involving an ordered distribution of cuprous and cupric ions in this proportion.

(ii) The thermal evolution of the magnetic susceptibilities excludes Cu^{2+}–Cu^{2+} magnetic interactions even at low temperature. In addition, the almost constant value of the TIP term is consistent with a constant crystal field at the Cu^{2+} site.

(iii) The low electronic conductivities exclude a hopping mechanism at long distance (Fig. 8).

(iv) The electronic microscopy experiments indicate the absence of extended defects or microdomains. At this scale a pseudo-cubic cell is observed with parameters which are twice those of an ideal perovskite. This result suggests a 1–1 copper–titanium ordering at short ranges. From these conclusions a model of copper–titanium cationic distribution can be proposed.

A cubic cluster of formal composition $La_8Cu_4Ti_4O_{24}$ is constructed. This cluster is made up of eight elementary groups $LaCu_{0.5}Ti_{0.5}O_3$ distributed equivalently over the three directions of the Cartesian space around one Cu^{2+} located at the center position (Fig. 9). Cu^{2+} is surrounded by 6 Cu^+ in type I or 6 Ti^{4+} in type II. The actual distribution in the long range order given by XRD would depend on the connection between two adjacent clusters. In addition, the vacancies are certainly associated with monovalent copper, which usually exhibits often linear or square planar oxygen coordination.

Obviously this interpretation leaves open more than one important question: the real Cu^+ coordination, the absence of static Jahn–Teller effect, etc. These are now under investigation.

REFERENCES

1. L. Monceaux and P. Courtine, *Eur. J. Inorg. Solid State Chem* **28,** (1) 233 (1991).
2. A. Serghini, M. Kacimi, M. Zyiad, and R. Brochu, *J. Chim. Phys.* **4,** 85 (1988).
3. M. L. Rojas, J. L. G. Fierro, L. G. Tejuca, and A. T. Bell, *J. Catal.* **124,** 41 (1990).
4. M. L. Rojas and J. L. G. Fierro, *J. Solid State Chem.* **89,** 299 (1990).
5. M. T. Anderson, V. E. Balbarin, D. A. Groenke, G. A. Bain, and K. R. Poeppelmeir, *J. Solid State Chem.* **103,** 216 (1993).
6. D. B. Wiles and R. Young, *J. Appl. Crystallogr.* **14,** 149 (1981).
7. P. A. Seinen, F. P. F. Van Berkel, W. A. Groen, and D. T. W. Ijdo, *Mater. Res. Bull.* **22,** 535, 1987.
8. W. A. Groen, F. P. F. Van Berkel, and D. J. W. Ijdo, *Acta Crystallogr. Sect. C* **42,** 1492 (1986).
9. M. Marezio and P. Dernier, *Mater. Res. Bull.* **6,** 23 (1971).
10. D. A. MacLean, H. N. Ng, and J. E. Greedan, *J. Solid State Chem.* **30,** 85 (1979).
11. P. Köhl and D. Reinen, *Z. Anorg. Allg. Chem.* **433,** 81 (1977).
12. P. Köhl, *Z. Anorg. Allg. Chem.* **442,** 280 (1978).